Probing the Mechanism of Aqueous Two-Phase System Formation for α-Elastin On-Chip

Yanjie Zhang, Hanbin Mao, and Paul S. Cremer*

Contribution from the Department of Chemistry, Texas A&M University, College Station, Texas 77843

Received August 11, 2003; E-mail: cremer@mail.chem.tamu.edu

Abstract: The kinetics of formation of the aqueous two-phase system (ATPS) for α-elastin was studied by dark field microscopy in an on-chip linear temperature gradient. Scattering intensities of protein solutions were recorded as a function of temperature and time, simultaneously at several concentrations. It was found that the formation rate of the ATPS could be fit as a first-order process and that the apparent rate constant increased with protein concentration. The activation energy for the process was 9.5 ± 0.5 kcal/mol, and this result was consistent with a coalescence mechanism. Experiments were also conducted with varying concentrations of sodium dodecyl sulfate, which shut off the coalescence mechanism forcing ATPS formation to proceed through Ostwald ripening. When this was done, the activation energy increased to 33 ± 2 kcal/mol and the kinetics became consistent with a second-order process.

Introduction

Aqueous two-phase systems (ATPS) are formed when two components in a water-based solution, which are mutually incompatible, separate into phases of different density under the force of gravity.[1-3] Examples of this phenomenon usually involve either two polymers (e.g., poly(ethylene glycol) and dextran) or a single polymer plus a high concentration of the appropriate salt.[4-7] The system phase separates such that one phase consists largely of the first component, whereas the second component predominates in the other. As each phase in the mixture is mostly water (75−90 wt %), the phase boundary has very low interfacial tension.[8] This fact has been widely exploited to separate proteins, amino acids, lipids, nucleic acids, and animal cells without significant interfacial denaturing effects which can be problematic when organic solvents are employed.[9-11] More recently, it has been shown that an aqueous solution containing only a single component can also lead to the formation of an ATPS.[12-14] In this case, the macromolecule

is thermoresponsive and begins to fold and form aggregates above its lower critical solution temperature (LCST). The particles in this cloudy solution then precipitate to form a clear viscous phase in which almost all of the polymeric material resides, while an upper less dense phase consists primarily of water (Figure 1). Such "one component" ATPSs may prove to be especially valuable in the isolation of cellular constituents because the need for additional separation steps can often be avoided. From a fundamental standpoint, probing the mechanistic details of ATPS formation for one-component systems may serve as a model for protein aggregation and related colloidal behavior.

Despite the fundamental and practical importance of one component ATPSs, the literature is almost completely devoid of information about the kinetics of their formation.[15] This paucity of information stems from the practical difficulties involved in making such measurements. First, it can be quite time-consuming to obtain data from coalescing and ripening particles in macroscopic test tubes because the time scale for ATPS formation is related to the dimensions of the tube in which the particles are settling.[16] Typical test tube heights are a few centimeters with diameters of about one centimeter. This leads to time scales of several hours or even tens of hours for ATPS formation to come to completion. Furthermore, it can be difficult to obtain reliable light scattering or adsorption information on species that are sinking to the bottom of the tube. Finally, it would be tedious to run a large series of experiments as a function of temperature, polymer concentration, and solvent conditions. These difficulties can be overcome by using tem-

(1) Sinha, J.; Dey, P. K.; Panda, T. *Appl. Microbiol. Biotechnol.* **2000**, *54*, 476−486.
(2) Hatti-Kaul, R. *Mol. Biotechnol.* **2001**, *19*, 269−277.
(3) Hatti-Kaul, R. *Methods Biotechnol. Vol 11, Aqueous Two-Phase Systems. Methods and Protocols* **2000**.
(4) Albertsson, P.-A. *Partition of Cell Particles and Macromolecules*; J. Wiley & Sons: New York, 1986.
(5) Ban, T.; Shibata, M.; Kawaizumi, F.; Nii, S.; Takahashi, K. *J. Chromatogr. B* **2001**, *76*, 65−72.
(6) Merchuk, J. C.; Andrews, B. A.; Asenjo, J. A. *J. Chromatogr. B* **1998**, *711*, 285−293.
(7) Baxter, S. M.; Sperry, P. R.; Fu, Z. *Langmuir* **1997**, *13*, 3948−3952.
(8) Jiang, J.; Prausnitz, J. M. *J. Phys. Chem. B* **2000**, *104*, 7197−7205.
(9) Walter, H.; Johansson, G. *Methods in Enzymology*, *Aqueous Two-Phase Systems*, **1994**, *228*.
(10) Persson, J.; Nyström, L.; Ageland, H.; Tjerneld, F. *J. Chromatogr. B* **1998**, *711*, 97−109.
(11) Li, M.; Zhu, Z.-Q.; Rodrigues, A. E. *Ind. Eng. Chem. Res.* **2002**, *41*, 251− 256.
(12) Johansson, H.-O.; Karlström, G.; Tjerneld, F. *Macromolecules* **1993**, *26*, 4478−4483.
(13) Johansson, H.-O.; Karlström, G.; Tjerneld, F. *Biochim. Biophys. Acta* **1997**, *1335*, 315−325.

(14) Johansson, H.-O.; Persson, J.; Tjerneld, F. *Biotechnol. Bioeng.* **1999**, *66*, 247−257.
(15) Salamanca, M. H.; Merchuk, J. C.; Andrews, B. A.; Asenjo, J. A. *J. Chromatogr. B* **1998**, *711*, 319−329.
(16) Solano-Castillo, C.; Rito-Palomares, M. *J. Chromatogr. B* **2000**, *743*, 195− 201.
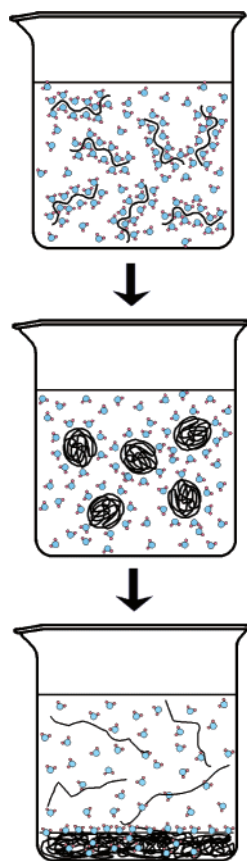
Figure 1. Schematic representation of "one component" ATPS formation.

perature gradient microfluidic techniques recently developed in our laboratory.[17−19] This is the case because the optical measurement is made in the same direction as the gravitational field, the heights involved are on the micron scale, and all temperature data are collected simultaneously. The experiment has the further advantage of requiring only a few microliters of solution. The technique works by positioning a microcapillary tube or microfluidic device in a dark field optical setup under a light microscope. Light-scattering information is gathered as a function of time over a range of temperatures by placing a linear temperature gradient across the sample. ATPS formation usually comes to completion in these devices in just a few minutes.

Using the microfluidic temperature gradient, we have explored the activation energy of ATPS formation for the thermoresponsive protein, α-elastin. Elastins are biomacromolecules that are responsible for maintaining the morphology of tissues such as artery walls, lungs, ligaments, and skin.[20−22] Elastin-related proteins and polypeptides (e.g., tropoelastin, α-elastin, and synthetic polypeptides with specific repeating amino acid sequences) undergo a two-stage reversible phase transitions in aqueous solutions above their LCST.[23−25] In the first stage, the

elastin-related polypeptides start out fully hydrated, and the solution is transparent. The protein forms coacervate droplets when the temperature is raised above the LCST due to the folding and aggregation of the biomolecules.[21] In the second stage, the suspension clears again with the formation of an ATPS upon standing.

The first stage of the phase transition for α-elastin, the LCST, has been investigated by various techniques including differential scanning calorimetry (DSC),[26−28] circular dichroism (CD),[29] light scattering,[30] transmission electron microscopy (TEM),[31] nuclear magnetic resonance (NMR),[32] and molecular dynamics simulations.[33] These studies suggest that α-elastin starts out in an extended conformation with tightly bound water molecules on the hydrophobic portions of the polypeptide. Above the LCST, these water molecules are released in a cooperative process which initiates the aggregation of the side chains. By contrast, far less is known about the aqueous two phase system formation, and no activation energy measurements are available. In fact, there seem to be few if any measurements of ATPS activation energies for any thermoresponsive systems in the literature.

The lack of information about ATPSs is unfortunate, as such data would undoubtedly aid in unraveling the mechanistic details of the process. Indeed, two major mechanistic pathways can be envisioned: Ostwald ripening and coalescence. The first involves the growth of particles through the transfer of monomers between them such that bigger particles grow at the expense of smaller ones. On the other hand, coalescence is the direct fusion of one particle with another to make a larger one. Each process has a separate activation barrier associated with it. In the case of Ostwald ripening, this should involve the desorption of single macromolecules from shrinking particles, whereas in the case of coalescence the barrier comes from the removal of intervening solvent molecules between the particles which are being joined. In the experiments presented below, we demonstrate that the apparent rate constants are consistent with a coalescence mechanism, although the process can be forced to proceed through Ostwald ripening by the addition of sodium dodecyl sulfate (SDS) to the solution.

Experimental Section

α-Elastin isolated from bovine neck ligament was purchased from Elastin Products Co., Inc. Low-conductivity H_2O, produced from a NANOpure Ultrapure Water System (Barnstead, Dubuque, IA) with a minimum resistivity of 18 MΩ·cm, was used to prepare sodium phosphate buffer solutions (10 mM, pH = 7.0). α-Elastin was dissolved in the buffer at concentrations ranging from 20 mg/mL to 40 mg/mL. This concentration range was chosen for investigation because a substantial change in the LCST can be observed over it. An additional

(17) Mao, H.; Yang, T.; Cremer, P. S. *J. Am. Chem. Soc.* **2002**, *124*, 4432−4435.
(18) Mao, H.; Holden, M. A.; You, M.; Cremer, P. S. *Anal. Chem.* **2002**, *74*, 5071−5075.
(19) Mao, H.; Li, C.; Zhang, Y.; Bergbreiter, D. E.; Cremer, P. S. *J. Am. Chem. Soc.* **2003**, *125*, 2850−2851.
(20) Lillie, M. A.; Gosline, J. M. *Biopolymers* **2002**, *64*, 127−138.
(21) Kaibara, K.; Watanabe, T.; Miyakawa, K. *Biopolymers* **2000**, *53*, 369−379.
(22) Li, D. Y.; Brooke, B.; Davis, E. C.; Mecham, R. P.; Sorensen, L. K.; Boak, B. B.; Eichwald, E.; Keating, M. T. *Nature* **1998**, *393*, 276−280.
(23) Urry, D. W. *J. Phys. Chem. B* **1997**, *101*, 11 007−11 028.
(24) Urry, D. W. *Angew. Chem., Int. Ed. Engl.* **1993**, *32*, 819−841.
(25) Urry, D. W. *Methods Enzymol.* **1982**, *82*, 673−717.
(26) Rodríguez-Cabello, J. C.; Alonso, M.; Pérez, T.; Herguedas, M. M. *Biopolymers* **2000**, *54*, 282−288.
(27) Wright, E. R.; McMillan, R. A.; Cooper, A.; Apkarian, R. P.; Conticello, V. P. *Adv. Funct. Mater.* **2002**, *12*, 149−154.
(28) Luan, C. H.; Parker, T. M.; Prasad, K. U.; Urry, D. W. *Biopolymers* **1991**, *31*, 465−475.
(29) Urry, D. W.; Long, M. M.; Cox, B. A.; Ohnishi, T.; Mitchell, L. W.; Jacobs, M. *Biochim. Biophys. Acta* **1974**, *371*, 597−602.
(30) Vrhovski, B.; Jensen, S.; Weiss, A. S. *Eur. J. Biochem.* **1997**, *250*, 92−98.
(31) Volpin, D.; Urry, D. W.; Cox, B. A.; Gotte, L. *Biochim. Biophys. Acta* **1976**, *439*, 253−258.
(32) Urry, D. W.; Trapane, T. L.; Sugano, H.; Prasad, K. U. *J. Am. Chem. Soc.* **1981**, *103*, 2080−2089.
(33) Li, B.; Alonso, D. O. V.; Daggett, V. *J. Mol. Biol.* **2001**, *305*, 581−592.

set of α-elastin samples was prepared with SDS at surfactant concentrations ranging from 1.0 to 2.2 mM.

Fabrication of the temperature gradient device has been described previously.[17−19] Briefly, a cover glass acting as a sample stage and heat conductor was mounted on top of two parallel brass tubes through which hot and cold antifreeze solutions could be individually flowed. Rectangular borosilicate capillary tubes (VitroCom, Inc.) with dimensions of 2 cm × 1 mm × 100 μm (length × width × height) were placed parallel to the temperature gradient. By employing rectangular capillary tubes, a constant temperature could be maintained throughout the same cross section of tubing. Light scattering from protein solutions was monitored via a CCD camera (Micromax 1024, Princeton Instruments) using dark field optics under an inverted microscope (Nikon, TE2000-U). Two different polymer solutions with previously measured LCSTs served to calibrate the slope of the gradient.[19] The first solution was 10 mg/mL poly (*N*-isopropyl acrylamide) (PNIPAM) in H$_2$O with a known LCST of 30.2 ± 0.2 °C and the other was 10 mg/mL PNIPAM in a 0.7 M KCl solution with a known LCST of 26.0 ± 0.2 °C. A single point calibration with only one PNIPAM solution was employed for all subsequent experiments as a control. Six rectangular capillary tubes could be fit side-by-side under a ×2 objective and time-lapse CCD images were taken every 5 s to follow the kinetics of ATPS formation. The temperature along the capillary tubes could be determined by counting the pixels in a linescan drawn along the temperature gradient in the CCD images. An absolute temperature calibration was made using thermocouple measurements as previously described.[17] All measurements reported in this manuscript have been taken a minimum of three times.

Results

Measuring the LCST of α-Elastin. Before investigating the kinetics of ATPS formation, measurements of the LCST of α-elastin were made. A series of five rectangular capillary tubes containing varying concentrations of α-elastin were placed along the direction of the linear temperature gradient in addition to a control tube. Dark field optics was used to observe the aggregation based on the simple principle that folded protein aggregates scatter significantly more light than soluble ones. Figure 2a shows a dark field image of capillary tubes containing α-elastin in phosphate buffer at concentrations ranging from 20 mg/mL to 40 mg/mL and temperatures from 24.0 °C to 48.1 °C. The image was taken almost immediately after being subjected to the temperature gradient. The areas inside the tubes which are dark represent little or no light scattering, whereas the purple regions designate a high degree of light scattering. The boundary between these two areas occurs at the lower critical solution temperature where the polymers begin to display aggregation behavior.

The systems evolved as a function of time (Figure 2b) as the ATPS formed. A linescan parallel to the temperature gradient was drawn across each sample and plotted out in Figure 2c,d. The width of the transition for the LCSTs was somewhat wider for elastin than for PNIPAM as the polypeptide samples have a higher polydispersity. The onset points of the LCST (T_b) in Figure 2a are plotted as a function of protein concentration in Figure 3. As can be seen, T_b decreased as the concentration of the elastin was raised in agreement with previous investigators.[25] Such results demonstrate the cooperativity of the LCST formation process as increased intermolecular interactions lead to a lowering of the transition temperature.

Kinetics of ATPS Formation in Phosphate Buffer. The onset of ATPS formation, as evidenced by a decrease in scattering intensity of precipitated α-elastin with time, began
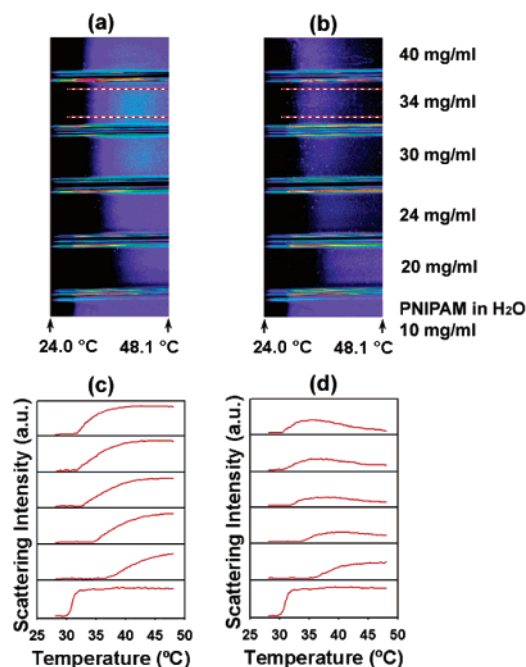
Figure 2. Dark field images at (a) $t = 0$ s and (b) $t = 100$ s of capillary tubes containing α-elastin at concentrations of 40, 34, 30, 24, and 20 mg/mL (from top to bottom). The very bottom tube contained a 10 mg/mL PNIPAM solution (LCST 30.2 °C) and served as an internal standard. (c) Linescans across each of the capillary tubes in (a). (d) Linescans across each of the capillary tubes from (b). Linescans are the average of the center 50 pixels across any given tube. These linescan widths are represented by dashed red lines in the 34 mg/mL data in the images above.
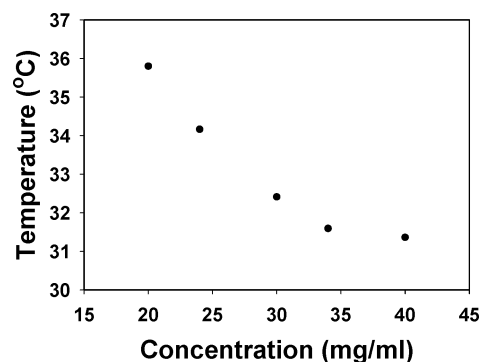

Figure 3. LCST values of α-elastin from Figure 2a as a function of concentration.

within seconds of the LCST formation. The image in Figure 2b was taken 100 s after that in Figure 2a. As can be seen, the amount of scattered light attenuated at all temperatures above the LCST. The endpoint of ATPS formation was judged to have occurred once no significant scattering from the precipitated elastin could be detected. The entire process was recorded by a time-lapse image series. As an example, the linescan from a sample with 30 mg/mL α-elastin is plotted against both temperature and time (Figure 4a). The scattering attenuated more rapidly at high temperature than at low temperature. At a given temperature, the decay of the scattering intensity as a function of time could be fit by a single-exponential decay function (eq 1)
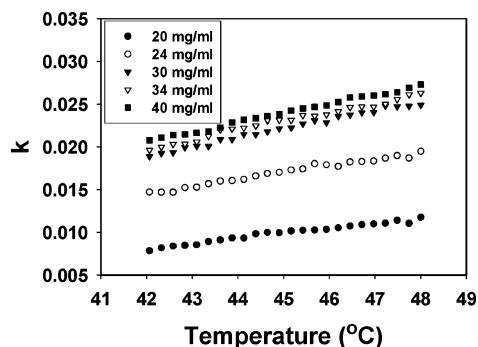
$$y = y_0 + ae^{-kt} \tag{1}$$

where y is the intensity of the scattered light, y_0 is the
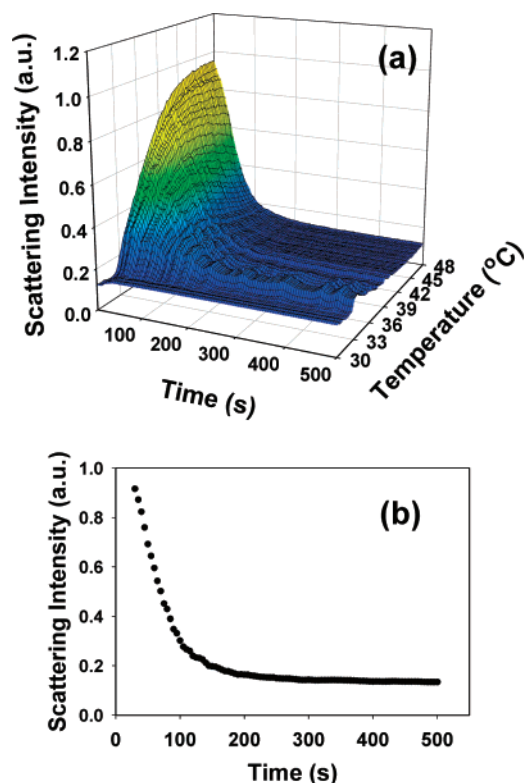
Figure 4. (a) Three-dimensional plot of light scattering intensity versus time and temperature of a 30 mg/mL α-elastin solution. (b) A curve fit from (a) at 44.1 °C.

Figure 5. (a) Apparent rate constant, k, for ATPS formation of α-elastin as a function of temperature at various protein concentrations.

background intensity, a is a proportionality factor, k is the apparent rate constant for the process, and t is time. A sample curve from this data set at 44.1 °C is shown in Figure 4b.

The above procedure allowed k to be determined as a function of temperature and concentration of α-elastin (Figure 5).[34] Two distinct phenomena are readily observable. First, k increased with increasing temperature. Second, at a given temperature k was larger when the α-elastin concentration was higher. The temperature dependence of the apparent rate constant could be fit by the Arrhenius equation (eq 2)

$$k = A \exp(-\Delta E/RT) \qquad (2)$$

Here, A is a prefactor, R is the gas constant, ΔE is the apparent

(34) Data were analyzed from the initially flatter portions of the intensity distribution (Figure 2c). This ensured that ATPS measurements were being taken from the portion of the tube where the vast majority of the polypeptides had undergone the LCST transition and, hence, the material which fell out of solution was uniform in composition.
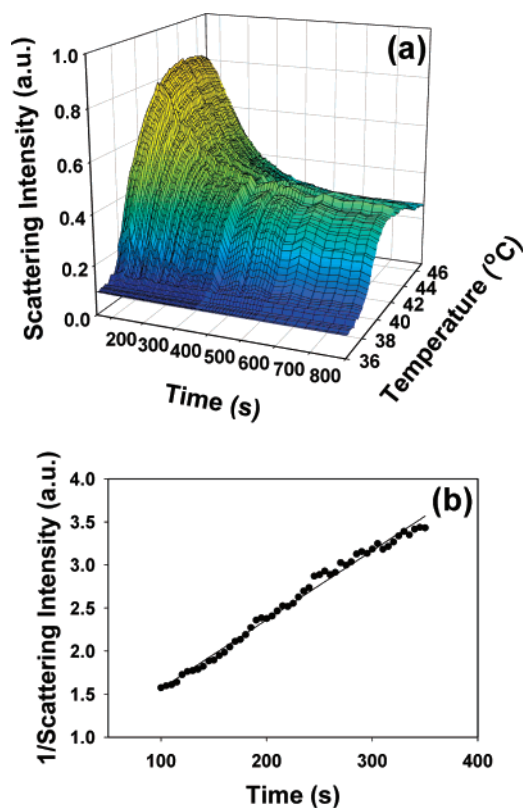
Figure 6. (a) Three-dimensional plot of light scattering intensity versus both time and temperature for a 27 mg/mL α-elastin solution with 2.0 mM SDS. (b) A curve fit from (a) at 44.6 °C.

activation energy, and T is the temperature in Kelvin. By plotting $\ln k$ versus $1/T$, ΔE can be obtained from the slope of the linear regression curve. The value of ΔE was determined to be 9.5 ± 0.5 kcal/mol regardless of the protein concentration over the range investigated.

ATPS Formation with SDS. To further probe the mechanism of ATPS formation, SDS was added to solutions containing 27 mg/mL α-elastin. It was found that when the concentration of SDS was 1.8 mM or greater, α-elastin could not fully complete the formation process even after several hours. Figure 6a shows an example of this case with an SDS concentration of 2.0 mM. Strikingly, the kinetics of scattering intensity attenuation followed second-order rather than first-order kinetics (eq 3)

$$\frac{1}{y} = kt + B \qquad (3)$$

Here, y stands for the light scattering intensity, B is a constant which represents the reciprocal of the scattering intensity at the onset of ATPS formation, k is the apparent rate constant and t is time. A sample-fitting curve for the SDS data at 44.6 °C is shown in Figure 6b. Again, k can be abstracted from the slope of the line. It should be noted that when the SDS concentration was 1.6 mM or below, the decay of the light scattering intensity could not be fit by eq 3 probably because the data were representative of a mixture of first and second-order kinetics. However, for solutions containing 1.8, 2.0, and 2.2 mM SDS, the kinetics were all well fit by the second-order equation.

Using the procedure described above, the apparent rate constant of ATPS formation could be determined both as a function of temperature and SDS concentration. A plot of $\ln k$
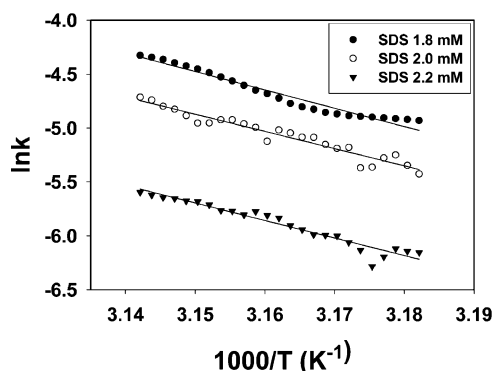
Figure 7. Arrhenius plots of ATPS formation for 27 mg/mL α-elastin at various SDS concentrations.

versus *1/T* for the data is shown in Figure 7. The ΔE values for ATPS formation in the presence of the three SDS concentrations mentioned above were 34 ± 2, 32 ± 2, and 32 ± 2 kcal/mol, respectively. In other words, the apparent activation energy maintained a nearly constant value once the SDS concentration exceeded 1.8 mM. Identical experiments were performed with SDS at different concentrations of α-elastin (30 and 40 mg/mL).[35] The activation energies were found to be the same as those reported with the 27 mg/mL samples within experimental error. The average value for all experiments was 33 ± 2 kcal/mol.

Discussion

At temperatures below the LCST, the nonpolar side-chains of α-elastin are surrounded by a large number of organized water molecules. After the temperature is raised above the LCST, these ordered water molecules are released into the bulk and aggregation of the side-chains leads to protein particle formation via hydrophobic interactions both intramolecularly and intermolecularly.[23] This behavior manifests itself in the turbidity of the solution due to light scattering by the coacervate droplets. At this stage, the individual droplets are still surrounded by ordered solvent molecules. Upon standing, however, the suspension forms an ATPS with the lower phase containing densely packed and folded α-elastin. On the other hand, the upper phase is mostly devoid of protein. The purpose here is to discuss the kinetics and mechanism of this second process.

Although the decay of the scattering intensity as a function of time could be well fit by a single-exponential decay function, ATPS formation is different from a standard first-order chemical reaction since the measured rate constant depends on the concentration of α-elastin. For an elementary reaction step, the rate constant must be independent of reactant concentration; however, for complex processes such as aggregation this need not be the case. Indeed, the LCST, which proceeds ATPS formation, is concentration dependent as the initial folding process can be either intermolecular or intramolecular.[23] At very low concentrations, it will be intramolecular, which has a higher activation barrier for LCST formation and slows this process down. At higher concentration, both pathways are active and

the process speeds up. This in turn causes the apparent rate constant for the subsequent ATPS step to appear to be concentration dependent because the two processes cannot be easily decoupled. Nevertheless, the apparent activation energy values obtained for ATPS formation are independent of concentration. In other words, the specific concentration of α-elastin chosen to measure the activation energy has no effect on the value of ΔE obtained.

As mentioned above, Ostwald ripening is the growth of large droplets in a dispersion at the expense of smaller ones. The solubility, *C*, of material decreases with increasing particle radius as can be shown through the Gibbs-Thompson equation (eq 4)[36−38]

$$C(r) = C_\infty \exp\left[\frac{2\gamma V_m}{rRT}\right] \approx C_\infty\left(1 + \frac{2\gamma V_m}{rRT}\right) \tag{4}$$

Here C_∞ is the solubility of the bulk material, γ is the surface tension, V_m is the molar volume of the material in the dispersed phase, r is the radius of a droplet, R is the gas constant, and T is the temperature in Kelvin. A decreasing concentration gradient in the radial direction extends out from the surface of sufficiently small droplets and an increasing gradient exists near larger droplets.[39] Such gradients ultimately lead to diffusive transfer of material from small droplets to larger ones. Throughout this process, the average droplet radius increases with time as sufficiently large ones release fewer and fewer soluble particles per unit surface area into the bulk.

Theoretically, the process of Ostwald ripening should be completed by the merger of all the particles into a single separate phase, but in practice this does not usually occur owing to a considerable decrease in the rate of the process as the average particle size increases.[40] The change in droplet number, *N*, in a system undergoing Ostwald ripening follows second-order kinetics (eq 5)[38,40]

$$\frac{1}{N_t} - \frac{1}{N_0} = k_2 t \tag{5}$$

On the other hand, for coalescence, two cases can be identified. First, in a very dilute solution, the collision rate between the droplets can be the rate-determining step. In that case, coalescence is a second-order process. At higher volume fractions of the dispersed phase, however, the rupture of the interfacial film between two droplets is the rate-determining step. Under these circumstances, which predominate at the concentrations employed in the present experiments, the kinetics of particle number attenuation become first order and follow the equation shown below[41,42]

$$N_t = N_0 \exp(-k_1 t) \tag{6}$$

It is generally thought that the coarsening of phase structure in undisturbed solutions of particles with reasonably high interfacial

(35) It should be noted that lower concentrations of α-elastin (i.e., 20 mg/mL) were also explored and should yield the same activation energy; however, the LCST of the polypeptide increases with increasing SDS concentration. This forces the ATPS formation processes to occur at higher temperatures. For the lowest sample concentrations this exceeds 60 °C. At that point, bubbles start to form near the hot end of the capillary tubes making experimental measurements difficult to analyze.

(36) Talapin, D. V.; Rogach, A. L.; Haase, M.; Weller, H. *J. Phys. Chem. B* **2001**, *105*, 12 278−12 285.
(37) Kabalnov, A. S.; Shchukin, E. D. *Adv. Colloid Interface Sci.* **1992**, *38*, 69−97.
(38) Taylor, P. *Adv. Colloid Interface Sci.* **1998**, *75*, 107−163.
(39) Fortelný, I.; Živný, A.; Jůza, J. *J. Polym. Sci. Part B, Polym. Phys.* **1999**, *37*, 181−187.
(40) Buscall, R.; Davis, S. S.; Potts, D. C. *Colloid & Polymer Sci.* **1979**, *257*, 636−644.
(41) Florence, A. T.; Rogers, J. A. *J. Pharm. Pharmac.* **1971**, *23*, 233−251.
(42) Buscall, R. *Prog. Colloid & Polymer Sci.* **1978**, *63*, 15−26.

tension is induced by coalescence, whereas Ostwald ripening may contribute in systems with a sufficiently low interfacial tension.[39] In the case of α-elastin, both the Ostwald ripening and coalescence mechanisms could potentially play important roles in the process of ATPS formation. The results without SDS reveal, however, that the process obeys first-order kinetics, which is consistent with a pure coalescence mechanism (Figure 4b). It therefore appears that the activation energy associated with coalescence is ~9.5 kcal/mol. This still leaves open the question of exactly how much higher the activation barrier would be for Ostwald ripening.

To explore the above point, ATPS formation was probed in the presence of SDS (Figure 6). Previous studies have suggested that anionic surfactants can shut off the coalescence pathway.[38,43–45] On the other hand, Ostwald ripening is not generally believed to be greatly affected by the presence of the surfactant. In the experiments presented above, it was found that with sufficient SDS, the kinetics switched quite obviously to second order and the apparent activation energy became nearly independent of SDS concentration. This is strong evidence that the dominant mechanism became Ostwald ripening. The fact that the ATPS could not come to completion also supports the conclusion that the formation pathway was Ostwald ripening rather than merely coalescence with a raised activation barrier. Therefore, the activation barrier for Ostwald ripening should be close to 33 ± 2 kcal/mol.

The above results indicate that the interfacial tension of coacervate droplets of α-elastin is sufficiently high to allow the entire ATPS process to ensue through coalescence with only a moderate activation barrier in the absence of surfactant. On the other hand, the interfacial tension is low enough in the presence of SDS that Ostwald ripening dominates. Now that a practical method is available for making such measurements, future studies can concentrate on determining how the apparent activation barrier is affected by the exact chemical composition of the elastin molecules. This can be best achieved by employing elastin-like polypeptides (ELPs) where the identity of particular amino acid residues can be systematically varied. Furthermore, the Ostwald ripening barrier in the presence of SDS could also be explored as a function of peptide chain length, residue identity, and solution conditions. Finally, it should be noted that these fundamental mechanistic studies are really only made possible through the employment of lab-on-a-chip devices. Indeed, the high-throughput capabilities and unique geometry of these platforms could be exploited for the investigation of a variety of aggregation experiments. It may also prove possible to exploit these devices for faster separation of cellular components.

JA037869C

(43) Soma, J.; Papadopoulos, K. D. *J. Colloid Interface Sci.* **1996**, *181*, 225–231.
(44) Smet, Y. D.; Deriemaeker, L.; Finsy, R. *Langmuir* **1999**, *15*, 6745–6754.
(45) Hoang, T. K. N.; La, V. B.; Deriemaeker, L.; Finsy, R. *Langmuir* **2002**, *18*, 10 086–10 090.